Hindawi
Advances in Materials Science and Engineering
Volume 2019, Article ID 8974625, 12 pages
https://doi.org/10.1155/2019/8974625

Research Article

The Mechanical Properties of Recycled Coarse Aggregate Concrete with Lithium Slag

Yongjun Qin,[1] **Jiejing Chen**,[1] **Zhenxing Li**,[1,2] **and Yabin Zhang**[1]

[1]*School of Architectural Engineering, Xinjiang University, Urumqi 830001, China*
[2]*School of Civil Engineering, Southeast University, Nanjing 210000, China*

Correspondence should be addressed to Yongjun Qin; 13144180978@163.com

Received 27 August 2019; Revised 14 November 2019; Accepted 2 December 2019; Published 31 December 2019

Academic Editor: Antonio Caggiano

Using recycled coarse aggregate (RCA) to replace natural pebbles and using lithium slag (LS) from industrial waste to replace cement in order to improve the mechanical properties of concrete and solve environmental problems. In this study, the effects of different substitution rates of RCA (0, 30%, 50%, and 70%) and different LS contents (0, 10%, 15%, 20%, and 25%) on the mechanical properties of concrete were investigated. The main results indicate that when the substitution rate of RCA is 30% and the LS content is 20%, optimal cube compressive strength, axial compressive strength, and elastic modulus can be achieved, with an increase of 9.90%, 48.22%, and 9.94% respectively; when the substitution rate of RCA is 70% and the LS content is 20%, the splitting tensile strength and flexural strength can be improved by 9.90% and 48.22%, respectively. The morphology of RCA concrete specimens with LS was observed with a scanning electron microscope (SEM). Moreover, corrections were made to improve the relevant formula according to the differences between the measured intensity index and data converted from current specifications.

1. Introduction

Due to the imbalance between economic and ecological development, more and more emphasis has been put on the concept of sustainable architecture in the field of civil engineering [1, 2]. With the growing investment in infrastructure construction in various countries and the rapid progress of revitalization and related reconstruction projects in old cities, the rising number of building demolitions has caused their materials to be abandoned in landfills.

This construction waste could be reused as recycled coarse aggregate [3]. Compared with natural aggregate, recycled aggregate has sharper edges, rougher surface, higher water absorption, and lower density, which will affect the strength characteristics of concrete [4]. Furthermore, with the rapid development of the lithium salt industry, emissions of lithium slag (LS) have become increasingly severe in China. It was reported that, in 2018, the global production of lithium salt was 329,000 tons, 250,500 tons of which was produced in China. Xinjiang is China's main lithium salt production base, accruing a large amount of LS that if not handled will cause serious environmental pollution [5–8]. So far, many scholars have conducted extensive research on recycled concrete or concrete containing LS. Safiuddina studied the main properties of RCA concrete [2], including old, new, and hardening properties; Tan et al. systematically studied concrete made with lithium slag's mechanical properties [6] and proved that LS could improve the compressive strength, dry shrinkage, creep, and other mechanical properties of concrete [8].

In order to improve the mechanical properties of concrete with RCA, more attention has been paid to ternary concrete such as recycled concrete containing fly ash, silica fume, or fiber [9–11]. In some countries, such ternary concrete containing RCA and fly ash could combine both of their advantages, accelerate the reaction speed of pozzolanic ash, and improve working performance and durability.

Based on the expectation that ternary mixture concrete may have greater development potential, LS is considered to be a suitable supplementary cementitious material for use in

recycled concrete [5, 12–15]. Some scholars found that the main components of LS are similar to that of nanosilica, blast furnace slag, and fly ash, which may explain its ability to improve the performance of concrete. According to the work of Ji, nanosilica with high pozzolanic activity could not only improve the density and strength of concrete but also improved its flexural capacity [16]. Xiao's research showed that the compressive strength of concrete could be improved by adding a suitable amount of fly ash [17], while Alireza et al. also proved that a ternary mixture of silica fume and fly ash required less water and had better durability than binary concrete only containing silica fume. Various studies have illustrated that recycled concrete with LS as a ternary mixture theoretically has more advantages over concrete with recycled aggregate or LS alone.

In the experiment, both natural coarse aggregate (NCA) and cement were replaced by RCA and LS at different substitution rates, respectively. The main contributions of this paper include the following: (1) studying the mechanical properties of a concrete mixture containing RCA and LS, including its cube compressive strength, axial compressive strength, splitting tensile strength, flexural strength, and modulus of elasticity, and (2) revising the relevant strength formula. This is an important field lacking prior investigation. Finally, the properties of recycled concrete mixed with LS are analyzed by SEM, which lays a foundation for future research in this field.

2. Materials and Methods

2.1. Materials. In this experiment, ordinary Portland cement (OPC) of grade 42.5 and LS were used, and the LS was provided by the lithium salt plant in Xinjiang. After dried and ground, the LS particle size was less than 45 μm. Table 1 shows the chemical composition of cement and LS.

According to the Chinese standard GB/T208-2014 [18], the specific gravities of cement and the LS were measured approximately 3000 kg/m^3 and 2450 kg/m^3, respectively. The specific surface areas of cement and the LS were 360 m^2/kg and 440 m^2/kg, respectively, based on measurement with the nitrogen adsorption test method. In addition, the LS particles had irregular shape according to the scanning electron microscopy (SEM). The local natural medium-coarse sand was used as the fine aggregate, with a fineness modulus of 2.9, an apparent density of 2640 kg/m^3, and a sand ratio of 38% [19]. The coarse aggregates were selected from local pebbles, and the particle size was adjusted to 5–20 mm continuous gradation after cleaned and screened. A municipal engineering waste in Xinjiang was selected as the source of recycled aggregate, and the waste was crushed, cleaned, and screened until the particle size was identical. The aggregate was classified as Class II according to the Chinese standard GB/T 25177-2010 [20]. The screening analysis of fine aggregate and coarse aggregate was carried out in accordance with the Chinese standard JGJ 52-2006 [21]. After the preparation, the physical properties of two kinds of coarse aggregate were tested according to the Chinese standard GBT 14685-2011 [22], as shown in Table 2. After being crushed, RCA had more edges and corners, rougher surface, higher porosity, and water absorption rate than NCA [2]. Due to cement paste adhesion and porous surface, they also presented great differences in other physical properties.

2.2. Preparation of Specimens. 375 specimens were prepared in total by using full permutation for the mixture design. The RCA substitution rates were set at 0, 30%, 50%, 70%, and 100%, respectively, and the LS contents were determined at 0, 10%, 15%, 20%, and 25%, respectively. The groups were named RCC (with RCA) and NCC (with NCA), respectively, for the convenience of comparison, and it is also easier to distinguish which experiment group contains RCA.

Considering the water absorption and moisture content of aggregate, the basic mix proportion of concrete was modified according to the Chinese standard DG/TJ 08-2018-2007 [23] before the preparation of concrete specimens. In previous experiments conducted by the team members, the appropriate additional water consumption was calculated. The specific mixing design of these five mixtures is presented in Table 3. In addition, the NCA and RCA should be kept in a dry state on the surface during the experiments.

The group with RCA substitution rate of 0 and LS content of 0 was set as the reference group, the remaining RCA and LS with different substitution rates were used as the research objects, and the water-cement ratio was maintained at 0.45. The RCA substitution rates were 0, 30%, 50%, 70%, and 100%, and LS was used as mixture with the content of 0, 10%, 15%, 20%, and 25%, respectively. A power-driven rotary mixer was employed for the preparation of specimens [24]. LS, cement, and aggregate were premixed for 2 minutes before adding water to achieve evener LS distribution in the mixture. The mixture was stirred before the vibration treatment and cured under the standard curing conditions.

2.3. Test Method

2.3.1. Measurement of Mechanical Properties. The cube compressive strength, axial compressive strength, splitting tensile strength, flexural strength, and elastic modulus of concrete were determined according to the Chinese standard GB/T 50081-2002 and GB/T 50152-2012 [25, 26]. Among them, the cube compressive and splitting tensile specimens had the dimension of 150 mm × 150 mm × 150 mm, the axial compressive and elastic modulus specimens had the dimension of 150 mm × 150 mm × 300 mm, and the flexural specimens had the dimension of 150 mm × 150 mm × 550 mm. Each design group included 25 sets, with 3 specimens in each set.

Tye-3000b press was used for loading, and the directional force control system was adopted to adjust the rate to be 0.5 MPa/s for cube compressive and axial compressive specimens, 0.05 MPa/s for splitting tensile and flexural specimens, and 0.6 MPa/s for elastic modulus specimens. At the same time, the relevant data were adjusted, and the corresponding deformations of the specimens were

Table 1: The chemical composition of cement and lithium slag/%.

Material	SiO_2	Al_2O_3	Fe_2O_3	CaO	MgO	SO_3	K_2O	Na_2O	Li_2O	Rest
Cement	21.22	5.05	3.26	60.24	0.97	2.67	0.50	0.73	—	2.13
Lithium slag	41.72	18.10	1.24	20.02	0.54	15.14	0.33	0.14	0.17	2.32

Table 2: Properties of coarse aggregate.

Type	Thickness density (kg/m^3)	Apparent density (kg/m^3)	Water absorption (%)	Crush value (%)	Mud content (%)	Fine powder content (%)
NCA	1536	2687	0.5	—	1	0.2
RCA	1472	2417	3.8	14	5.2	0.4

Note: NCC represents natural concrete; RCC represents recycled concrete.

Table 3: The design of mix proportion.

Code	RCA (%)	LS (%)	Mix proportion ($kg \cdot m^{-3}$)						
			Water	Additional water	Cement	LS	NCA	RCA	Sand
NCC-0-0	0	0	195.00	0.00	433.00	0.00	1221.40	0.00	523.50
NCC-0-10	0	10	195.00	0.00	389.70	43.30	1221.40	0.00	523.50
NCC-0-15	0	15	195.00	0.00	368.05	64.95	1221.40	0.00	523.50
NCC-0-20	0	20	195.00	0.00	346.40	86.60	1221.40	0.00	523.50
NCC-0-25	0	25	195.00	0.00	324.75	108.25	1221.40	0.00	523.50
RCC-30-0	30	0	195.00	7.84	433.00	0.00	854.98	366.42	523.50
RCC-50-0	50	0	195.00	13.07	433.00	0.00	610.70	610.70	523.50
RCC-70-0	70	0	195.00	18.30	433.00	0.00	366.42	854.98	523.50
RCC-100-0	100	0	195.00	26.13	433.00	0.00	0.00	1221.40	523.50
RCC-30-10	30	10	195.00	7.84	389.70	43.30	854.98	366.42	523.50
RCC-30-15	30	15	195.00	7.84	368.05	64.95	854.98	366.42	523.50
RCC-30-20	30	20	195.00	7.84	346.40	86.60	854.98	366.42	523.50
RCC-30-25	30	25	195.00	7.84	324.75	108.25	854.98	366.42	523.50
RCC-50-10	50	10	195.00	13.07	389.70	43.30	610.70	610.70	523.50
RCC-50-15	50	15	195.00	13.07	368.05	64.95	610.70	610.70	523.50
RCC-50-20	50	20	195.00	13.07	346.40	86.60	610.70	610.70	523.50
RCC-50-25	50	25	195.00	13.07	324.75	108.25	610.70	610.70	523.50
RCC-70-10	70	10	195.00	18.30	389.70	43.30	366.42	854.98	523.50
RCC-70-15	70	15	195.00	18.30	368.05	64.95	366.42	854.98	523.50
RCC-70-20	70	20	195.00	18.30	346.40	86.60	366.42	854.98	523.50
RCC-70-25	70	25	195.00	13.07	324.75	108.25	366.42	854.98	523.50
RCC-100-10	100	10	195.00	26.13	389.70	43.30	0.00	1221.40	523.50
RCC-100-15	100	15	195.00	26.13	368.05	64.95	0.00	1221.40	523.50
RCC-100-20	100	20	195.00	26.13	346.40	86.60	0.00	1221.40	523.50
RCC-100-25	100	25	195.00	13.07	324.75	108.25	0.00	1221.40	523.50

Note: in NCC/RCC-50-10, NCC represents natural concrete; RCC represents recycled concrete; 50 represents RCA 50% substitution rate; 10 represents LS 10% content; other specimen numbers are set according to this method.

measured with pressure gauge and percentile meter. The flexural loading mode, elastic modulus loading device, and system are shown in Figure 1 in detail. In the elastic modulus loading system, it was necessary to conduct frequent loading and unloading to reduce error. Since concrete is an elastoplastic body, the elastic stage can be restored after loading, but the plastic stage cannot. Plastic strain energy is continuously consumed at each loading and unloading until only elastic strain energy is left, at which point the slope is a relatively accurate elastic modulus.

2.3.2. Microscopic Observation. Microstructures of NCC-0-0, RCC-30-20, RCC-30-10, and RCC-70-20 in the experimental groups were observed by SEM in order to determine the modification and effect of recycled concrete mixed with LS. The experiment specimens which were obtained from the fracture after compressive strength experiment were dried in a vacuum chamber to eliminate the interference of moisture on the observation results before scanning electron microscopy. A layer of conductive coating sparing could be used to gain a clearer observation image on the sample [27]. Specimens were detected under high vacuum conditions. All pictures could be taken by adjusting voltage and resolution.

3. Experimental Discussions

3.1. Test Data. It should be pointed out that the linear slope from the origin to the tangent point of the stress-strain curve of a prism is the elastic modulus of concrete under static

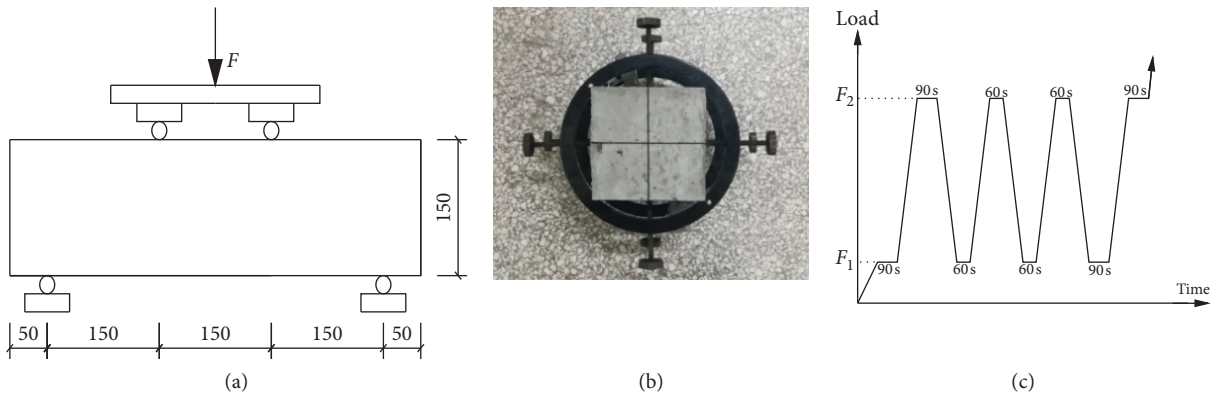

Figure 1: (a) Flexural loading method, (b) elastic modulus device, and (c) elastic modulus loading system.

pressure. According to the related requirement in the current standard of China, the elastic modulus of concrete can be calculated according to the formula, and the elastic modulus and compressive performance change synchronously. It is indicated that the elastic modulus of concrete is positively correlated to its strength, which is within the range from 3.01×10^4 MPa to 3.54×10^4 MPa, and this can meet the requirements of elastic modulus of C30 ordinary concrete (3×10^4 MPa). According to the previous experiment, the cubic strength of concrete would reach the maximum value in 28 d which can be used as an experimental reference. The specific data of the experiment specimens are shown in Table 4.

3.2. Analysis of Mechanical Properties

3.2.1. Cube Compressive Strength and Axial Compressive Strength. Figures 2 and 3 show the curves of the cube compressive strength and the axial compressive strength under the effect of RCA and LS.

Tests illustrate a consistent influence trend of the RCA substitution rate and LS content on the cube compressive strength and axial compressive strength of concrete, with the extreme values appearing at RCA substitution rate of 30% and LS content of 20%. Both the cube compressive strength and the axial compressive strength of the specimens present a trend of increase-decrease, with peak values for cube and axial compressive strength showing an increase of 18.84% and 18.85%, respectively, with an RCA content of 30% compared with ordinary concrete.

Obviously, both RCA and LS have their optimal prescribed amount, above which will cause degradation of mechanical properties of concrete. The compressive strength increases linearly and sharply with the addition of RCA before the optimal substitution rate is obtained. Possible explanations for this increase are that the surface roughness of recycled aggregate can increase the bond of cement aggregate, and the high water absorption capacity of recycled aggregate can reduce the water-cement ratio of the interface transition zone and improve the strength of the cement slurry [28].

Table 4: Test data.

Code	f_{cu} (MPa)	f_c (MPa)	$f_{t,s}$ (MPa)	f_f (MPa)	E_c (10^4 MPa)
NCC-0-0	35.56	27.85	3.20	2.84	3.02
NCC-0-10	37.90	30.36	4.11	3.76	3.10
NCC-0-15	39.90	32.65	4.30	3.94	3.16
NCC-0-20	41.84	34.87	4.41	4.04	3.21
NCC-0-25	36.73	29.11	3.80	3.48	3.06
RCC-30-0	42.26	32.7	3.85	3.53	3.25
RCC-50-0	39.58	29.32	3.57	3.27	3.14
RCC-70-0	37.41	27.1	3.36	3.08	3.07
RCC-100-0	34.89	25.8	3.10	2.93	2.94
RCC-30-10	45.40	36.12	4.29	3.93	3.39
RCC-30-15	46.99	38.23	4.43	4.06	3.49
RCC-30-20	49.75	41.28	4.54	4.16	3.54
RCC-30-25	43.97	34.41	4.01	3.67	3.35
RCC-50-10	41.90	32.39	4.43	4.06	3.24
RCC-50-15	45.03	35.5	4.63	4.24	3.35
RCC-50-20	46.49	37.65	4.75	4.35	3.41
RCC-50-25	40.63	30.86	4.19	3.84	3.20
RCC-70-10	40.66	30.96	4.58	4.19	3.15
RCC-70-15	43.67	33.9	5.04	4.34	3.26
RCC-70-20	45.35	36.09	4.91	4.50	3.32
RCC-70-25	39.39	29.03	4.33	3.96	3.12
RCC-100-10	35.63	28.48	3.99	3.65	3.06
RCC-100-15	37.91	31.19	4.20	3.84	3.13
RCC-100-20	39.33	33.20	4.32	3.96	3.18
RCC-100-25	34.70	27.14	3.64	3.33	3.01

Note. f_{cu}: cube compressive strength; f_c: axial compressive strength; $f_{t,s}$: splitting tensile strength; f_f: flexural strength; E_c: elastic modulus.

Moreover, excessive RCA may cause the influence of microcracks in concrete to be greater than the effect of secondary curing. With the increase of LS content, the cube compressive strength and axial compressive strength of concrete are similarly enhanced before decreasing, with peak strength occurring when the content of LS is 20%. With an LS content of 20%, the cube compressive strength and axial compressive strength increase by 17.36% and 17.44%, respectively, when compared with specimens of the same RCA substitution rate and LS content of 0. This phenomenon is attributed to the fact an increase in LS will change the internal structure of the concrete, improve the water retention and adhesion of the concrete, optimize the porosity, and

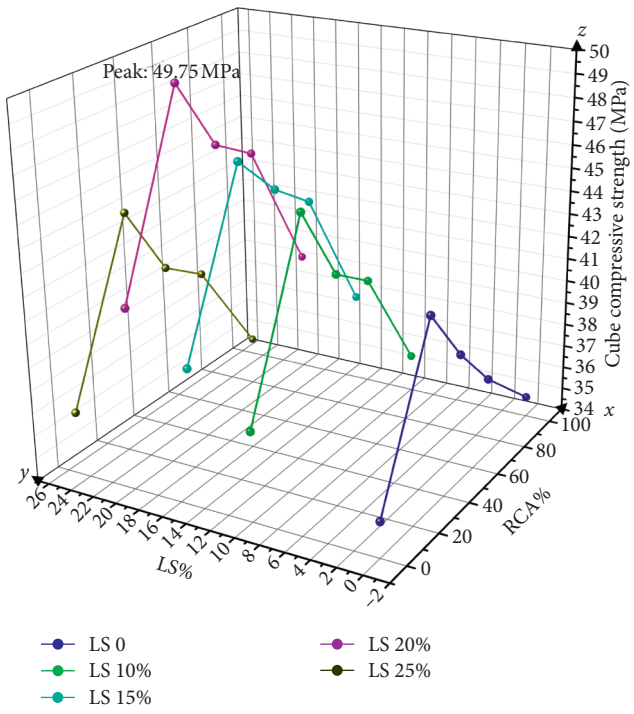

Figure 2: The effect of RCA and LS on the cube compressive strength.

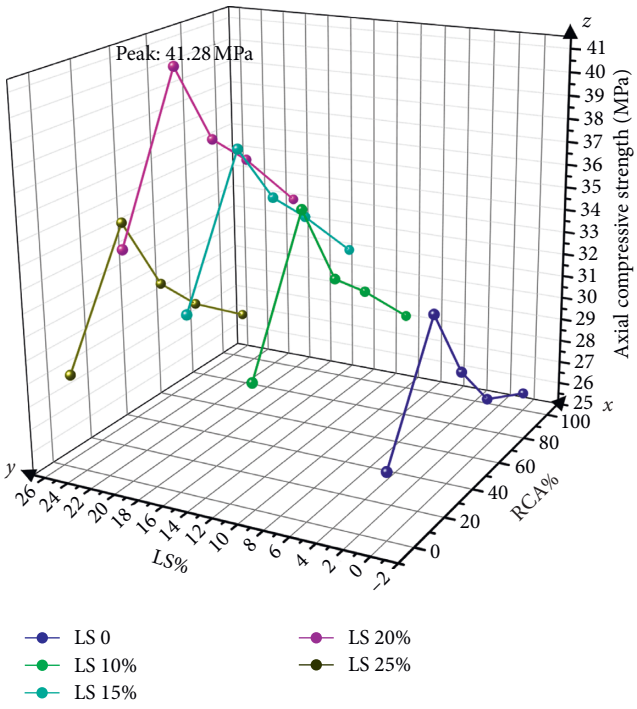

Figure 3: The effect of RCA and LS on the axial compressive strength.

improve its compactness [29, 30]. When the content of LS is higher than 20%, only a small amount of hydration products (C-S-H) will be generated with the increase of LS, which cannot effectively stimulate its pozzolanic reaction. The porosity of the concrete will increase, and the compactness and compressive strength will show a downward trend as the rest of the LS only plays the role of filler. In fact, the size of the pores in concrete is crucial to the compressive strength, and the more developed the pores, the lower the compressive strength.

Wagih et al.'s results indicated that the optimum percentage of RCA was between 25% and 50% [31]. Wu demonstrated that the compressive strength keeps increasing when the content of LS is less than 20% [32]. Xiao et al. found that when the substitution rate of RCA reached 30%, the decrease of compressive strength of concrete could be neglected [33]. All of their conclusions are consistent with the results of our experiment. The maximum compressive strength appears when the RCA substitution rate is 30% and the content of LS is 20%.

3.2.2. Splitting Tensile Strength and Flexural Strength. The splitting tensile strength and flexural strength of concrete with different contents of LS and different RCA substitution rates are shown in Figures 4 and 5.

Obviously, without LS, the splitting tensile strength and flexural strength of the specimens would firstly increase and then decrease with the increase of RCA. The peak values appear at the RCA substitution rate of 30%. The splitting tensile strength and flexural strength are 20.31% and 24.07% higher than those of ordinary concrete, respectively. It is found by Andreu and Miren that the use of 20% RCA can make a 3%~22% increase in the splitting tensile strength, which is almost consistent with the result in this paper [28]. However, after the addition of LS, the peak values of splitting tensile strength and flexural strength of specimens with an RCA substitution rate of 70% are greatly different from those without LS.

With the increase of LS, the tensile strength and flexural strength of the specimens firstly increase and then decrease. There is a special case, namely, as the RCA substitution rate is 70% with an LS content of 15%, the maximum tensile strength can be obtained. Except for this, the peak value for the RCA substitution rate appears when the LS content is 20%. More specially, without the LS, the splitting tensile strength with an RCA substitution rate of 100% decreases by about 10%, compared with an RCA substitution rate of 0, which is almost consistent with the findings of Grdic et al. [34]. In their study, tensile strength is weakened for the concrete with the RCA substitution rate of 100%. The flexural strength of the concrete with an RCA substitution rate of 100% is even higher than that without RCA. Because RCA can improve the strength of cement slurry, the flexural strength may be related to the cement slurry.

3.2.3. Elastic Modulus. Figure 6 shows the curve of the elastic modulus under the effects of RCA and LS.

With the same content of LS, the elastic modulus of the specimens will firstly increase and then decrease with the increase of RCA, and the peak appears at a 30% RCA substitution rate, which is 9.43% higher than that of the specimens with the RCA substitution rate of 0. In general,

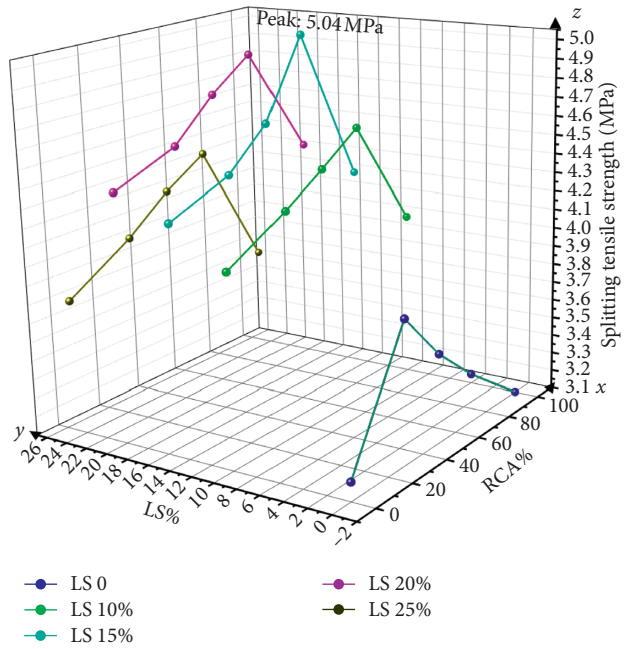

Figure 4: The effect of RCA and LS on the splitting tensile strength.

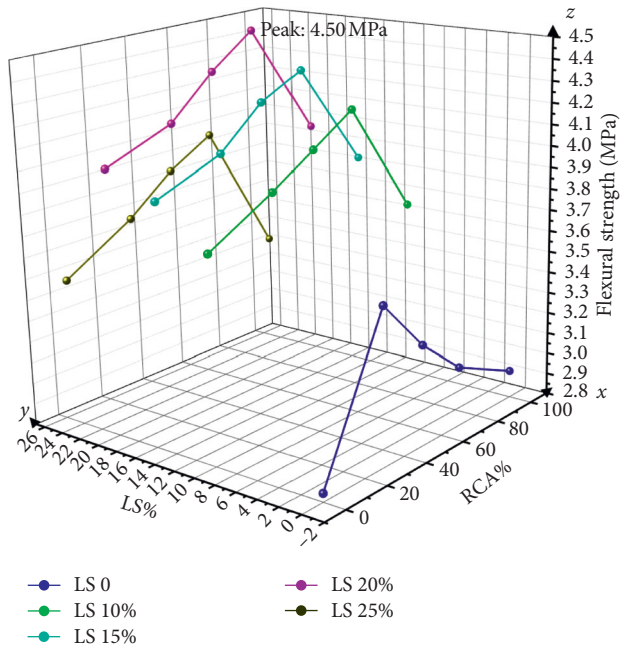

Figure 5: The effect of RCA and LS on the flexural strength.

the greater the strength is, the greater the modulus of elasticity is, so the apparent modulus of elasticity curve is more consistent with that of the compressive strength curve. In Figure 6, without the addition of LS, the elastic modulus of the 100% substitution rate of RCA is lower than that of the substitution rate of 0. This suggests that the elastic modulus of composite aggregate has a greater impact on the elastic modulus of concrete at this time. RCA has larger pores and smaller strength, which directly leads to the lower elastic modulus of concrete.

Under the same RCA substitution rate, the elastic modulus of the specimen firstly increases and then decreases with the gradual addition of LS. The peak value appears when the content of LS is 20%, which is about 8.02% higher than the specimens with the same RCA substitution rate and 0 LS content. Xie et al. found that the formula between porosity and the modulus of elasticity agreed well with each other through the backscattered electrons and nanoindentation, which indicated that the denser the microstructure was, the greater the modulus of elasticity was in the same region [35].

The secondary pozzolanic reaction of LS produces more hydration products (C-S-H) to fill the pores, thus causing the uptrend of the elastic modulus [8]. However, it is not suitable to add more LS after the extreme point, because too much LS will result in an excessive paste, which is not conducive to the elastic modulus. Based on the influence curve of RCA and LS on the elastic modulus, it can be found that the combined peak value of the two occurs at the same values, where the substitution rate of RCA is 30% and the content of LS is 20%. It is well known that the elastic modulus not only reflects the deformation performance of concrete but is also a function of compressive strength. It is reasonable that the influence curve of elastic modulus coincides with that of compressive strength. Based on the comprehensive experimental analysis, 30% RCA substitution rate and 20% LS content will make concrete with excellent working performance, thus laying a foundation for future research.

3.3. Microscopic Analysis. After a number of experiments, the optimal mix proportion of 30% RAC and 20% LS was determined by adjusting the proportion of LS and RCA in the mix. SEM is an intuitive way to investigate the internal interface trauma and the products after chemical reaction occurs in the concrete, so as to make the research more reliable. The main components of lithium slag are active SiO_2 and Al_2O_3, which is the same as fly ash, slag, and even nano-SiO_2 [36, 37]. Its pozzolanic properties can make the active SiO_2 and Al_2O_3 react with the hydration product Ca $(OH)_2$ of cement through an activation process, which will result in the secondary hydration of cementitious materials to form gel substances such as calcium silicate hydrate, calcium aluminate hydrate, and calcium silicate hydrate. They can fill the microporous structure in the pore walls of hardened slurry and improve the compressive strength. Four groups of NCC-0-0, RCC-30-20, RCC-30-10, and RCC-70-20 were selected for comparison.

SEM pictures of the concrete microstructures with different LS contents and RCA substitution rates of RCA are as follows. The internal microstructure is loose with many pores in NCC-0-0 [8]. In Figure 7(a), a large number of Ca $(OH)_2$ lamellar crystals appear with a consistent orientation because of the incomplete hydration reaction, which is not conducive to compressive and cracking strength. The existence of Ca $(OH)_2$ usually indicates a weak link in the concrete. It can be seen from

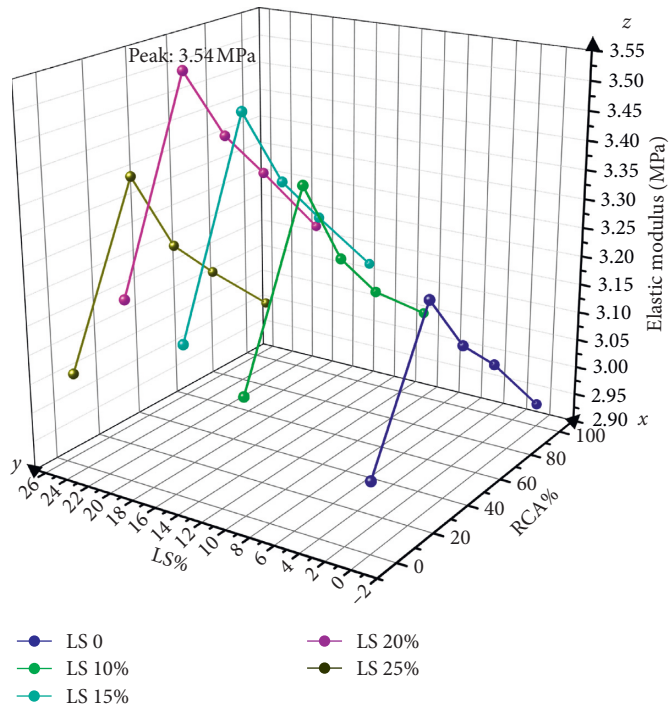

Figure 6: The effect of RCA and LS on the elastic modulus.

Figures 7(b) and 7(c) that the specimens with 30% RCA and the specimens with 10% RCA are more compact than the natural aggregate concrete experimental specimens in their internal microstructure, and their holes to some extent are fewer. However, Figure 7(b) shows more dispersed internal morphology and more holes than Figure 7(c), so it is not difficult to prove that, compared with NCC-0-10, RCC-30-0 has a denser internal structure with better performance. In Figure 7(d), the microstructure is obviously improved and the structure becomes more compact after the addition of 30% RCA and 10% LS. The concrete presents a fine and uniform continuum, and a good spatial network skeleton structure is formed between the hydration products and the aggregate [38, 39]. Active SiO_2, Al_2O_3, and Ca $(OH)_2$ are hydrated twice with the mix proportion of LS to form hydrated calcium silicate and calcium aluminate with cementitious properties [5]. At this time, there are very small capillary pores in the specimens, which are surrounded or filled by hydration products (C-S-H). Moreover, the consumption of Ca $(OH)_2$ makes the reaction go forward and accelerates the hydration of cement, so the compressive strength is further enhanced.

It is found by observing the microstructure of RCC-30-20 that the internal interface morphology is relatively regular [40, 41]. As shown in Figure 8(a), Ca $(OH)_2$ crystals with irregular shapes are present in an ordered arrangement. In addition, Ca $(OH)_2$ mostly deposits in the hydration products (C-S-H), and the number of Ca $(OH)_2$ significantly decreases under high resolution [42]. The aggregate matches well with cement paste with a dense internal surface, which is attributed to the generated gel. The internal particles form an amorphous porous microstructure, which makes the network microstructure of the material and the colloidal structure tight and complete. The images under SEM indicate that LS has a microaggregate effect, which can fill internal gap between cement particles, increase compactness, and reduce porosity. After the 30% RCA and 25% LS are added, the microstructure significantly improves and is generally as dense as that with the best proportion. But Figure 8(b) shows that there are many gaps between LS and the surrounding gel, which indicates that LS has not been fully utilized, mainly because not enough Ca $(OH)_2$ is produced by hydration to support the development of the secondary hydration. As a result, the unreacted LS particles increase the porosity and reduce the compressive strength.

The compressive strength of the specimens with 70% RCA and 20% LS significantly decreases, compared with the specimens with the ideal proportions. From its microstructure in Figure 9, there are many obvious slits in the specimen's microstructure with relatively obvious voids and inefficient fills. Substances are dispersed from one another, and it is difficult to find the gels that play a binding role in the high-resolution images. This is because the RCA has strong water absorption ability, resulting in a lower water-cement ratio as well as inadequate hydration of cement in the surrounding area of the aggregate. Thus, the microstructure of hydration products (C-S-H) correspondingly decreases, which is not conducive to filling and bonding.

The mechanical properties are reflected in the microstructure. The internal structures of LS and RCA with different substitution rates are different, so their mechanical properties are different. SEM intuitively illustrates the accuracy and reliability of the experimental results, which lays

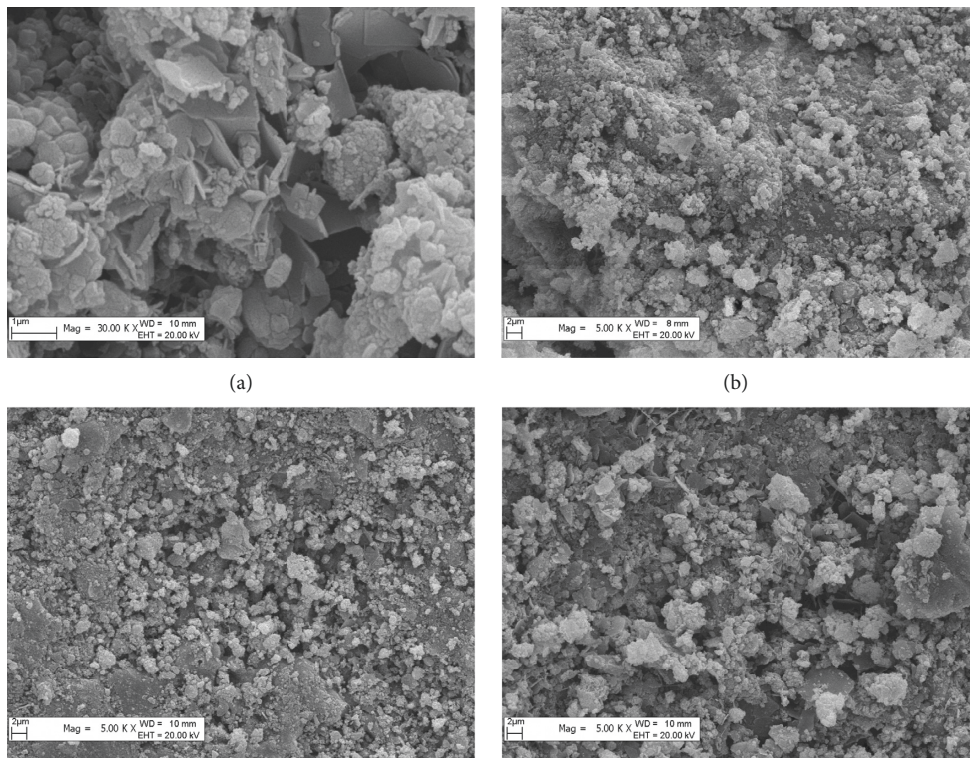

Figure 7: Microstructure of NCC-0-0, RCC-30-10, RCC-30-10, and RCC-30-10 in the experimental group. Magnification of the microstructure of (a) NCC-0-0, (b) NCC-0-10, (c) RCC-30-0, and (d) RCC-30-10.

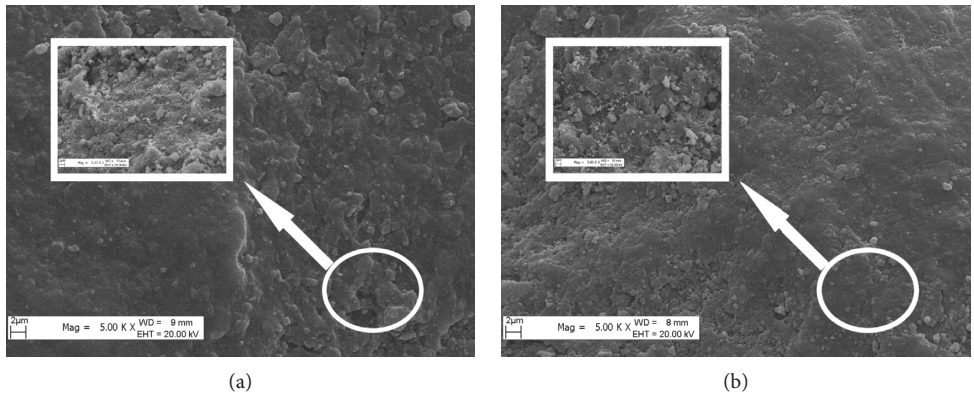

Figure 8: Pore enlargement of (a) RCC-30-20 and (b) RCC-30-25 in the experimental group.

the foundation for future research on related materials or microstructures.

3.4. Correction of the Relevant Formula. Tables 4 and 5 illustrate the related data in the experiment.

3.4.1. Correction of Compressive Strength Formula. The current Chinese standard GB50010-2010 [43] takes a factor of 0.76 for the safety consideration of ordinary concrete:

$$f_c^1 = 0.76 f_{cu}. \quad (1)$$

From Table 5, it can be seen that the calculated value calculated by equation (1) is significantly smaller than the measured value f_c^1, the average difference is −3.816%, and the average value is about 0.790, which makes the actual axial pressure ratio different from the specification.

Based on the data of f_c and f_{cu} in Table 4, and after regression analysis, the relationship between the cubic compressive strength and the axial compressive strength of

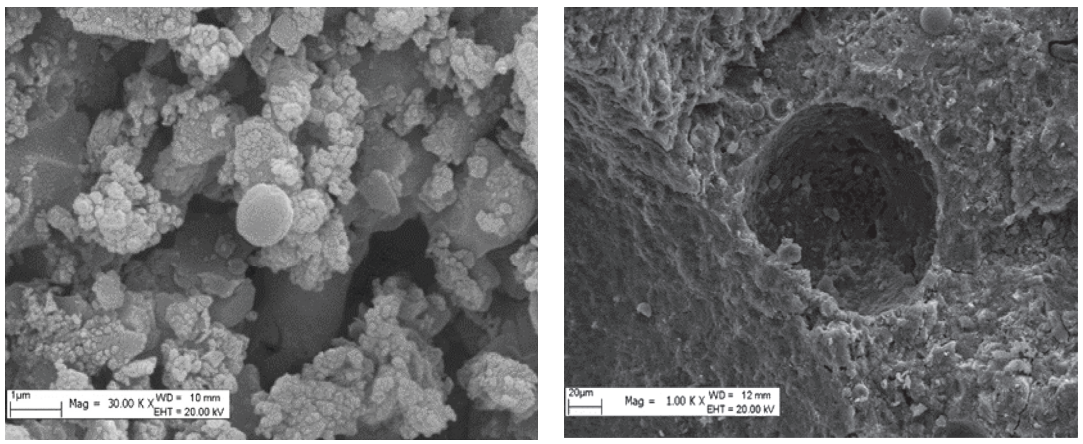

(a) (b)

Figure 9: Microstructure of RCC-70-20 in the experimental group.

Table 5: Calculation data.

Code	f_c^1 (MPa)	f_c^2 (MPa)	$f_{t,s}^1$ (MPa)	$f_{t,s}^2$ (MPa)	f_f^1 (MPa)	f_f^2 (MPa)	E_c^1 (10^4 MPa)	E_c^2 (10^4 MPa)
NCC-0-0	27.03	27.42	2.77	3.68	4.47	3.36	3.15	2.98
NCC-0-10	28.80	29.53	2.90	3.89	4.62	3.56	3.21	3.10
NCC-0-15	30.32	31.33	3.02	4.07	4.74	3.72	3.26	3.18
NCC-0-20	31.80	33.08	3.13	4.25	4.85	3.88	3.30	3.26
NCC-0-25	27.91	28.48	2.83	3.79	4.55	3.46	3.18	3.04
RCC-30-0	32.12	33.46	3.15	4.28	4.88	3.91	3.31	3.27
RCC-50-0	30.08	31.04	3.00	4.04	4.72	3.70	3.25	3.17
RCC-70-0	28.43	29.09	2.87	3.85	4.59	3.52	3.20	3.07
RCC-100-0	26.52	26.82	2.73	3.62	4.43	3.31	3.13	2.94
RCC-30-10	34.50	36.29	3.32	4.56	5.05	4.15	3.37	3.38
RCC-30-15	35.71	37.72	3.41	4.69	5.14	4.27	3.40	3.42
RCC-30-20	37.81	40.21	3.56	4.93	5.29	4.47	3.45	3.49
RCC-30-25	33.42	35.00	3.24	4.43	4.97	4.04	3.35	3.33
RCC-50-10	31.84	33.14	3.13	4.25	4.85	3.88	3.30	3.26
RCC-50-15	34.22	35.96	3.30	4.52	5.03	4.13	3.37	3.37
RCC-50-20	35.33	37.27	3.38	4.65	5.11	4.24	3.39	3.41
RCC-50-25	30.88	31.99	3.06	4.14	4.78	3.78	3.27	3.21
RCC-70-10	30.90	32.02	3.06	4.14	4.78	3.78	3.28	3.21
RCC-70-15	33.19	34.73	3.23	4.41	4.96	4.02	3.34	3.32
RCC-70-20	34.47	36.25	3.32	4.55	5.05	4.15	3.37	3.37
RCC-70-25	29.94	30.87	2.99	4.03	4.71	3.68	3.25	3.16
RCC-100-10	27.08	27.48	2.77	3.69	4.48	3.37	3.15	2.98
RCC-100-15	28.81	29.53	2.90	3.89	4.62	3.56	3.21	3.10
RCC-100-20	29.89	30.82	2.98	4.02	4.70	3.68	3.24	3.16
RCC-100-25	26.38	26.65	2.72	3.60	4.42	3.29	3.13	2.93

the experiment specimens is obtained as follows. The fit curve of the equations is shown in Figure 10.

$$f_c^2 = 0.90142 f_{cu} - 4.63373. \quad (2)$$

3.4.2. Modification of Splitting Tensile Strength Formula. At present, for ordinary concrete, the conversion formula between splitting tensile strength $f_{t,s}$ and cubic compressive strength f_{cu} is generally taken as follows[43]:

$$f_{t,s}^1 = 0.19 f_{cu}^{3/4}. \quad (3)$$

To organize and analyze the data in the table, it is recommended that the relationship between the tensile strength of the specimen and the compressive strength of the cube is shown in equation (4). The fit curves of two equations are attached in Figure 11.

$$f_{t,s}^2 = 0.29918 f_{cu}^{0.75} - 0.67628. \quad (4)$$

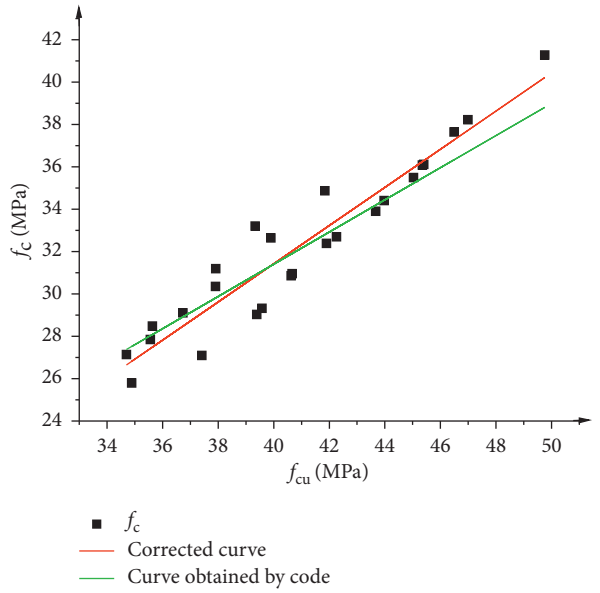

Figure 10: Curves of equation.

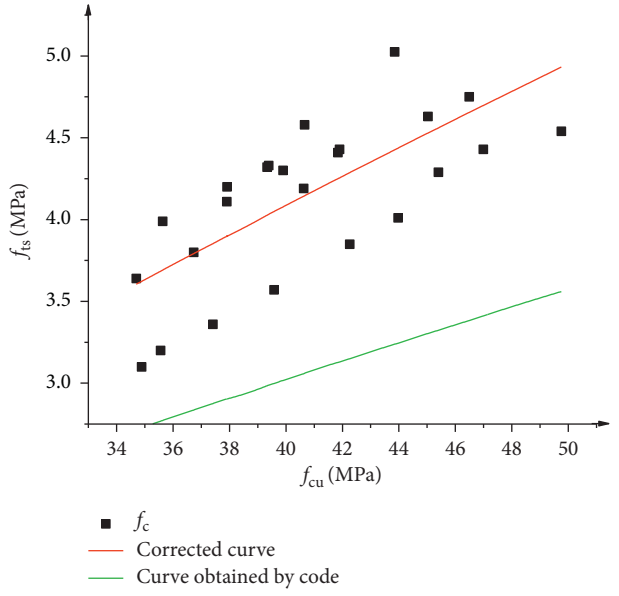

Figure 11: Curves of equation.

3.4.3. Modification of the Formula of Flexural Strength. For the flexural strength, Zheren [44] found that there is a certain relationship between the compressive and flexural strength of concrete cubes. The relationship between the two proposed by the Chinese standard DG/TJ 08-2018-2007 [23] is given by

$$f_f^1 = 0.75 f_{cu}^{0.5}. \tag{5}$$

It can also be seen from Table 5 that the calculated value f_f^1 according to formula (5) has a large volatility. After analyzing the data in the table, the relationship between the compressive strength and the flexural strength of the experiment specimen is obtained as follows. And the curves of equations are shown in Figure 12.

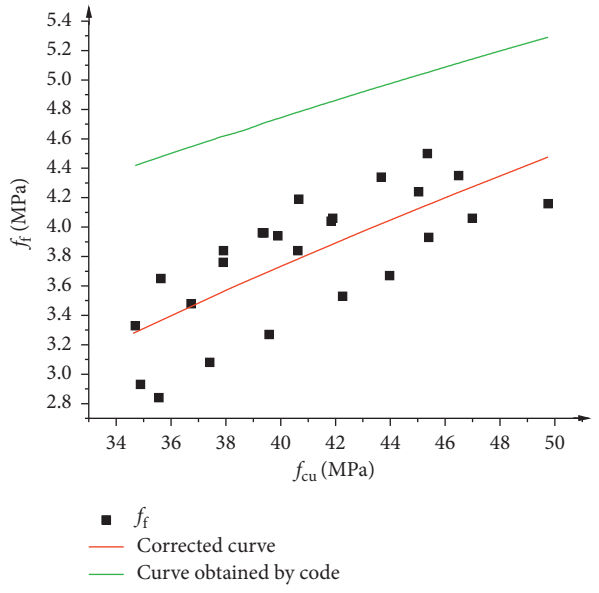

Figure 12: Curves of equation.

$$f_f^2 = 1.0193 f_{cu}^{0.5} - 2.71468. \tag{6}$$

3.4.4. Modification of Elastic Modulus Formula. The elastic modulus of concrete could reflect the deformation capacity of the experiment specimen, so the relationship between the two proposed by the current design specification [43] is given by

$$E_c^1 = \frac{10^5}{2.2 + (34.7/f_{cu})}. \tag{7}$$

The relevant data of the elastic modulus of the experiment specimen measured by the test are shown in Table 5 which could be seen that the calculated value E_c^1 of equation (7) was more discrete than the measured value E_c^2. After data processing and analysis, the relationship between the flexural strength of the specimen and the cubic compressive strength is given by

$$E_c^2 = \frac{10^5}{2.2 + (34.7/1.57455 f_{cu} - 25.93526)}. \tag{8}$$

The curves of equations are shown in Figure 13.

4. Conclusion

(1) When the LS is not incorporated, the cube compression, axial compression, splitting tensile strength, flexural strength, and elastic modulus of the experimental specimens with 30% RCA substitution rate are 42.26 MPa, 32.7 MPa, 3.85 MPa, 3.53 MPa, and 3.25 MPa, respectively. Moreover, they are 18.84%, 18.85%, 20.31%, 24.07%, and 7.62% higher, respectively, compared with ordinary concrete, showing an optimal performance.

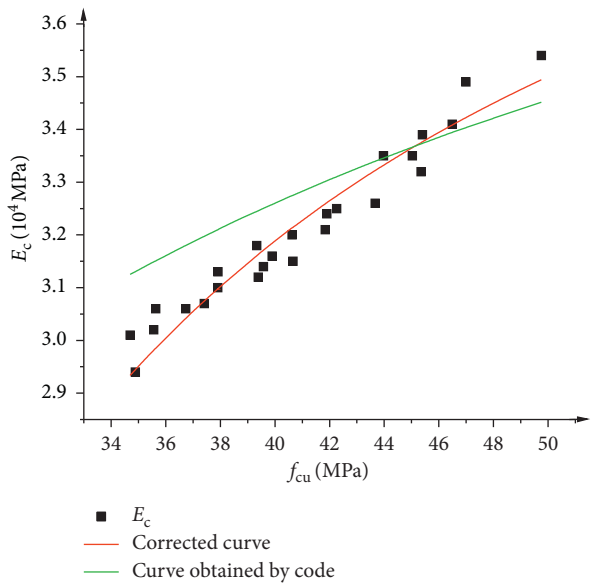

Figure 13: Curves of equation.

(2) When the RCA is not incorporated, the cube compression, axial compression, splitting tensile strength, flexural strength and elastic modulus of experimental specimens with 20% content are 36.73 MPa, 29.11 MPa, 3.80 MPa, 3.48 MPa, and 3.06 MPa, respectively. Moreover, they are 17.36%, 17.44, 34.82%, 34.84%, and 8.02% higher, respectively, compared with ordinary concrete, showing the optimal performance.

(3) When RCA and LS are added at the same time, experimental specimens with the proportion of 30% RCA and the content of 20% LS show the optimal cube compressive strength, axial compressive strength, and elastic modulus at 9.75 MPa, 41.28 MPa, and 4.54 MPa, respectively, which are 39.90%, 48.22%, and 9.94% higher compared with ordinary concrete. When the experimental specimens with the proportion of 30% RCA and the content of 20% LS, the splitting tensile strength and bending strength of concrete are 4.16 MPa and 3.54 MPa, respectively, which are 46.48% and 17.22% higher than those of ordinary concrete.

(4) Microscopic examination shows that the appropriate addition of LS can promote the development of gel structure and improve the microstructure of recycled concrete. However, the aperture of concrete would increase after exceeding the optimal content.

(5) After the gap between the measured strength index and the data in the current code is corrected, the relevant formula is more practical.

Data Availability

The data used to support the findings of this study are available from the corresponding author upon request.

Conflicts of Interest

The authors declare that there are no conflicts of interest regarding the publication of this paper.

Acknowledgments

The work described in this paper was fully supported by a grant from the Natural Science Foundation of China (study on the performance and constitutive relation of recycled concrete with lithium slag as mineral admixture), China (project no. 51668061).

References

[1] A. K. Padmini, K. Ramamurthy, and M. S. Mathews, "Influence of parent concrete on the properties of recycled aggregate concrete," *Construction and Building Materials*, vol. 23, no. 2, pp. 829–836, 2009.

[2] M. D. Safiuddin, U. J. Alengaram, A. Salam, M. Z. Jumaat, F. F. Jaafar, and H. B. Saad, "Properties of high-workability concrete with recycled concrete aggregate," *Materials Research*, vol. 14, no. 2, pp. 248–255, 2011.

[3] M. Ahmadi, A. Farzin, A. Hassani, and M. Motamedi, "Mechanical properties of the concrete containing recycled fibers and aggregates," *Construction and Building Materials*, vol. 144, pp. 392–398, 2017.

[4] A. Bagheri, H. Zanganeh, H. Alizadeh, M. Shakerinia, and M. A. S. Marian, "Comparing the performance of fine fly ash and silica fume in enhancing the properties of concretes containing fly ash," *Construction and Building Materials*, vol. 47, pp. 1402–1408, 2013.

[5] Z.-h. He, S.-g. Du, and D. Chen, "Microstructure of ultra high performance concrete containing lithium slag," *Journal of Hazardous Materials*, vol. 353, pp. 35–43, 2018.

[6] H. Tan, X. Li, C. He, B. Ma, Y. Bai, and Z. Luo, "Utilization of lithium slag as an admixture in blended cements: physico-mechanical and hydration characteristics," *Journal of Wuhan University of Technology-Materials Science Edition*, vol. 30, no. 1, pp. 129–133, 2015.

[7] F. F. Wu, K. B. Shi, and S. K. Dong, "Properties and microstructure of HPC with lithium-slag and fly ash," *Key Engineering Materials*, vol. 599, pp. 70–73, 2014.

[8] Z.-h. He, L.-y. Li, and S.-g. Du, "Mechanical properties, drying shrinkage, and creep of concrete containing lithium slag," *Construction and Building Materials*, vol. 147, pp. 296–304, 2017.

[9] V. Radonjanin, M. Malešev, S. Marinković, and A. E. S. Al Malty, "Green recycled aggregate concrete," *Construction and Building Materials*, vol. 47, pp. 1503–1511, 2013.

[10] B. González-Fonteboa and F. Martínez-Abella, "Concretes with aggregates from demolition waste and silica fume. Materials and mechanical properties," *Building and Environment*, vol. 43, no. 4, pp. 429–437, 2008.

[11] C. V. Umadevi and M. R. Gowda, "Study on strength characteristics of recycled aggregate concrete using polypropylene fiber," *Journal of Civil Engineering Technology and Research*, vol. 2, no. 1, pp. 259–266, 2014.

[12] W. Yiren, W. Dongmin, C. Yong, Z. Dapeng, and L. Ze, "Micro-morphology and phase composition of lithium slag from lithium carbonate production by sulphuric acid process," *Construction and Building Materials*, vol. 203, pp. 304–313, 2019.

[13] Y. Qiu, D. Wu, L. Yan, and Y. Zhou, "Recycling of spodumene slag: preparation of green polymer composites," *RSC Advances*, vol. 6, no. 43, pp. 36942–36953, 2016.

[14] F. F. Wu, G.-q. Wang, K.-b. Shi, J. Hao, and C. Zhai, "The comprehensive utilization of lithium slag," *Fly Ash Comprehensive Utilization*, vol. 3, pp. 46–50, 2012, in Chinese.

[15] L. Zhang, S. Z. Lv, Y. Liu, S. Y. Xiao, and P. S. Zhou, "Influence of lithium slag on cement properties," *Journal of Wuhan University of Technology*, vol. 37, no. 3, pp. 23–27, 2015.

[16] T. Ji, "Preliminary study on the water permeability and microstructure of concrete incorporating nano-SiO_2," *Cement and Concrete Research*, vol. 35, no. 10, pp. 1943–1947, 2005.

[17] L. Xiao and D. Jiang, "The effect of fly ash on the mechanical properties of cinder lightweight aggregate concrete," *IOP Conference Series: Earth and Environmental Science*, vol. 61, p. 012116, 2017.

[18] Quality Inspection Press of China, *GB/T 208-2014 Test Method for Determining Cement Density*, Quality Inspection Press of China, Beijing, China, 2014, in Chinese.

[19] X. W. Luo, H. L. Yao, and Z. Lu, "Production of recycled concrete and its material properties," *Materials Research Innovations*, vol. 19, no. sup1, pp. S1–S147, 2015.

[20] Standards Press of China, *GB/T 25177-2010 Recycled Coarse Aggregate for Concrete*, Standards Press of China, Shanghai, China, 2010, in Chinese.

[21] China Architecture & Building Press, *JGJ 52-2006 Technical Requirements and Test Method Standards for Ordinary Concrete Sandstone*, China Architecture & Building Press, Beijing, China, 2006, in Chinese.

[22] Standards Press of China, *GBT 14685-2011 Pebble and Crushed Stone for Construction*, Standards Press of China, Shanghai, China, 2011, in Chinese.

[23] Shanghai Construction and Traffic Committee, *DG\TJ 08-2018-2007 The Technical Code on the Application of Recycled Concrete*, Shanghai Construction and Traffic Committee, Shanghai, China, 2007, in Chinese.

[24] H. Liu, X. Wang, Y. Jiao, and T. Sha, "Experimental investigation of the mechanical and durability properties of crumb rubber concrete," *Materials*, vol. 9, no. 3, p. 172, 2016.

[25] China Architecture & Building Press, *GB/T 50081-2002 The Standard for Test Method of Mechanical Properties on Ordinary Concrete*, China Architecture & Building Press, Beijing, China, 2003, in Chinese.

[26] China Architecture & Building Press, *GB/T 50152-2012 Standard for Test Method of Concrete Structure*, China Architecture & Building Press, Beijing, China, 2012, in Chinese.

[27] X. F. Wang, Y. J. Huang, G. Y. Wu et al., "Effect of nano-SiO_2 on strength, shrinkage and cracking sensitivity of lightweight aggregate concrete," *Construction and Building Materials*, vol. 175, pp. 115–125, 2018.

[28] G. Andreu and E. Miren, "Experimental analysis of properties of high performance recycled aggregate concrete," *Construction and Building Materials*, vol. 52, pp. 227–235, 2014.

[29] L. Qi, H. Shaowen, Z. Yuxuan, L. Jinyang, P. Weiliang, and W. Yufeng, "Influence of lithium slag from lepidolite on the durability of concrete," *IOP Conference Series: Earth and Environmental Science*, vol. 61, p. 012151, 2017.

[30] A. Heidari and D. Tavakoli, "A study of the mechanical properties of ground ceramic powder concrete incorporating nano-SiO_2 particles," *Construction and Building Materials*, vol. 38, pp. 255–264, 2013.

[31] A. M. Wagih, H. Z. El-Karmoty, M. Ebid, and S. H. Okba, "Recycled construction and demolition concrete waste as aggregate for structural concrete," *HBRC Journal*, vol. 9, no. 3, pp. 193–200, 2013.

[32] F. Wu, L. Chen, K. Shi et al., "Properties and microstructure of HPC with lithium slag," *Journal of Engineering Science and Technology*, vol. 15, no. 12, pp. 219–222, 2015.

[33] J. Z. Xiao, J. B. Li, Z. P. Sun, and X. Hao, "Study on compressive strength of recycled aggregate concrete," *Journal of Tongji University*, vol. 32, pp. 1558–1561, 2004.

[34] Z. J. Grdic, G. A. Toplicic-Curcic, I. M. Despotovic, and N. S. Ristic, "Properties of self-compacting concrete prepared with coarse recycled concrete aggregate," *Construction and Building Materials*, vol. 24, no. 7, pp. 1129–1133, 2010.

[35] Y. Xie, D. J. Corr, F. Jin, H. Zhou, and S. P. Shah, "Experimental study of the interfacial transition zone (ITZ) of model rock-filled concrete(RFC)," *Cement and Concrete Composites*, vol. 55, pp. 223–231, 2015.

[36] C. Jaturapitakkul, K. Kiattikomol, V. Sata, and T. Leekeeratikul, "Use of ground coarse fly ash as a replacement of condensed silica fume in producing high-strength concrete," *Cement and Concrete Research*, vol. 34, no. 4, pp. 549–555, 2004.

[37] F. U. A. Shaikh and S. W. M. Supit, "Mechanical and durability properties of high volume fly ash (HVFA) concrete containing calcium carbonate ($CaCO_3$) nanoparticles," *Construction and Building Materials*, vol. 70, pp. 309–321, 2014.

[38] M. Ltifi, A. Guefrech, P. Mounanga, and A. Khelidj, "Experimental study of the effect of addition of nano-silica on the behavior of cement mortars," *Procedia Engineering*, vol. 10, pp. 900–905, 2011.

[39] T. Meng, Y. Yu, and Z. Wang, "Effect of nano-$CaCO_3$ slurry on the mechanical properties and micro-structure of concrete with and without fly ash," *Composites Part B: Engineering*, vol. 117, pp. 124–129, 2017.

[40] H.-J. Lee, J. H. Lee, and D. G. Kim, "Study on the change in microstructure of fly ash concrete depending on ages and degree of hydration using XRD and SEM," *Advanced Materials Research*, vol. 486, pp. 350–355, 2012.

[41] A. Al Ghabban, A. B. Al Zubaidi, Z. Jafar, and Z. Fakhri, "Effect of nano SiO_2 and nano $CaCO_3$ on the mechanical properties, durability and flowability of concrete," *IOP Conference Series: Materials Science and Engineering*, vol. 454, p. 012016, 2018.

[42] G. Constantinides and F.-J. Ulm, "The effect of two types of C-S-H on the elasticity of cement-based materials: results from nanoindentation and micromechanical modeling," *Cement and Concrete Research*, vol. 34, no. 1, pp. 67–80, 2004.

[43] China Architecture & Building Press, *GB50010-2010 Code for Design of Concrete Structure*, China Architecture & Building Press, Beijing, China, 2010, in Chinese.

[44] D. Zheren, *Principle and Application of Reinforced Concrete Nonlinear Finite Element Method*, China Water Power Press, Beijing, China, 2002, in Chinese.